ARTICLE

Mutations in *KLHL40* Are a Frequent Cause of Severe Autosomal-Recessive Nemaline Myopathy

Gianina Ravenscroft,[1,28] Satoko Miyatake,[2,28] Vilma-Lotta Lehtokari,[3,4] Emily J. Todd,[1] Pauliina Vornanen,[3,4] Kyle S. Yau,[1] Yukiko K. Hayashi,[5] Noriko Miyake,[2] Yoshinori Tsurusaki,[2] Hiroshi Doi,[2] Hirotomo Saitsu,[2] Hitoshi Osaka,[6] Sumimasa Yamashita,[6] Takashi Ohya,[7] Yuko Sakamoto,[7] Eriko Koshimizu,[2] Shintaro Imamura,[8] Michiaki Yamashita,[8] Kazuhiro Ogata,[9] Masaaki Shiina,[9] Robert J. Bryson-Richardson,[10] Raquel Vaz,[10] Ozge Ceyhan,[11] Catherine A. Brownstein,[11] Lindsay C. Swanson,[11] Sophie Monnot,[12] Norma B. Romero,[13] Helge Amthor,[12] Nina Kresoje,[14] Padma Sivadorai,[15] Cathy Kiraly-Borri,[16] Goknur Haliloglu,[17] Beril Talim,[17] Diclehan Orhan,[18] Gulsev Kale,[18] Adrian K. Charles,[19] Victoria A. Fabian,[15] Mark R. Davis,[15] Martin Lammens,[20] Caroline A. Sewry,[21] Adnan Manzur,[21] Francesco Muntoni,[21] Nigel F. Clarke,[22] Kathryn N. North,[23] Enrico Bertini,[24] Yoram Nevo,[25] Ekkhard Willichowski,[26] Inger E. Silberg,[27] Haluk Topaloglu,[17] Alan H. Beggs,[11] Richard J.N. Allcock,[14] Ichizo Nishino,[5] Carina Wallgren-Pettersson,[3,4] Naomichi Matsumoto,[2,29,*] and Nigel G. Laing[1,29,*]

Nemaline myopathy (NEM) is a common congenital myopathy. At the very severe end of the NEM clinical spectrum are genetically unresolved cases of autosomal-recessive fetal akinesia sequence. We studied a multinational cohort of 143 severe-NEM-affected families lacking genetic diagnosis. We performed whole-exome sequencing of six families and targeted gene sequencing of additional families. We identified 19 mutations in *KLHL40* (kelch-like family member 40) in 28 apparently unrelated NEM kindreds of various ethnicities. Accounting for up to 28% of the tested individuals in the Japanese cohort, *KLHL40* mutations were found to be the most common cause of this severe form of NEM. Clinical features of affected individuals were severe and distinctive and included fetal akinesia or hypokinesia and contractures, fractures, respiratory failure, and swallowing difficulties at birth. Molecular modeling suggested that the missense substitutions would destabilize the protein. Protein studies showed that KLHL40 is a striated-muscle-specific protein that is absent in *KLHL40*-associated NEM skeletal muscle. In zebrafish, *klhl40a* and *klhl40b* expression is largely confined to the myotome and skeletal muscle, and knockdown of these isoforms results in disruption of muscle structure and loss of movement. We identified *KLHL40* mutations as a frequent cause of severe autosomal-recessive NEM and showed that it plays a key role in muscle development and function. Screening of *KLHL40* should be a priority in individuals who are affected by autosomal-recessive NEM and who present with prenatal symptoms and/or contractures and in all Japanese individuals with severe NEM.

[1]Western Australian Institute for Medical Research and the Centre for Medical Research, University of Western Australia, Nedlands, Western Australia 6009, Australia; [2]Department of Human Genetics, Yokohama City University Graduate School of Medicine, Yokohama 236-0004, Japan; [3]The Folkhälsan Institute of Genetics, Samfundet Folkhälsan, Biomedicum Helsinki, PB 63 (Haartmaninkatu 8), University of Helsinki, Helsinki 00014, Finland; [4]Department of Medical Genetics, Haartman Institute, University of Helsinki, Helsinki 00014, Finland; [5]Department of Neuromuscular Research, National Institute of Neuroscience, National Center of Neurology and Psychiatry, Tokyo 187-8502, Japan; [6]Division of Neurology, Clinical Research Institute, Kanagawa Children's Medical Center, Yokohama 232-8555, Japan; [7]Department of Pediatrics, Odawara Municipal Hospital, Odawara 232-8558, Japan; [8]National Research Institute of Fisheries Science, Yokohama 236-8648, Japan; [9]Department of Biochemistry, Yokohama City University Graduate School of Medicine, Yokohama 236-0004, Japan; [10]School of Biological Sciences, Monash University, Victoria 3800, Australia; [11]The Manton Center for Orphan Disease Research, Genetics and Genomics, Boston Children's Hospital and Harvard Medical School, Boston MA, 02115, USA; [12]Service Génétique Médicale, Hôpital Necker-Enfants Malades, Université Paris Descartes, Paris 75015, France; [13]Unité de Morphologie Neuromusculaire, Institut de Myologie, Institut National de la Santé et de la Recherche Médicale, Paris 75651, France; [14]Lotterywest State Biomedical Facility Genomics and School of Pathology and Laboratory Medicine, University of Western Australia, Perth, Western Australia 6000, Australia; [15]Department of Anatomical Pathology, Royal Perth Hospital, Perth, Western Australia 6000, Australia; [16]Genetic Services of Western Australia, Princess Margaret Hospital for Children and King Edward Memorial Hospital for Women, Subiaco, Western Australia 6008, Australia; [17]Department of Pediatric Neurology, Hacettepe University Children's Hospital, Ankara 06100, Turkey; [18]Department of Pediatric Pathology, Hacettepe University Children's Hospital, Ankara 06100, Turkey; [19]School of Women's and Infants' Health, University of Western Australia, Crawley, Western Australia 6009, Australia; [20]Department of Pathology, University Hospital Antwerp, Antwerp 2650, Belgium; [21]Dubowitz Neuromuscular Centre, UCL Institute of Child Health and Great Ormond Street Hospital for Children, London WC1N 1EH, UK; [22]Institute for Neuroscience and Muscle Research, Children's Hospital at Westmead, Sydney 2145, Australia; [23]Murdoch Childrens Research Institute, The Royal Children's Hospital, Parkville, Victoria 3052, Australia; [24]Unit of Neuromuscular Disorders, Bambino Gesù Children's Hospital, Rome, Lazio 00165, Italy; [25]Neuropediatric Unit, Hadassah Medical Center, Hebrew University of Jerusalem, Jerusalem 91240, Israel; [26]Department of Pediatrics and Pediatric Neurology, University Medicine Göttingen, Göttingen 37075, Germany; [27]Neonatal Intensive Care Unit, Department of Pediatric Research, Women and Children's Division, Oslo University Hospital Rikshospitalet, Oslo 0424, Norway
[28]These authors contributed equally to this work
[29]These authors contributed equally to this work
*Correspondence: nigel.laing@uwa.edu.au (N.G.L.), naomat@yokohama-cu.ac.jp (N.M.)
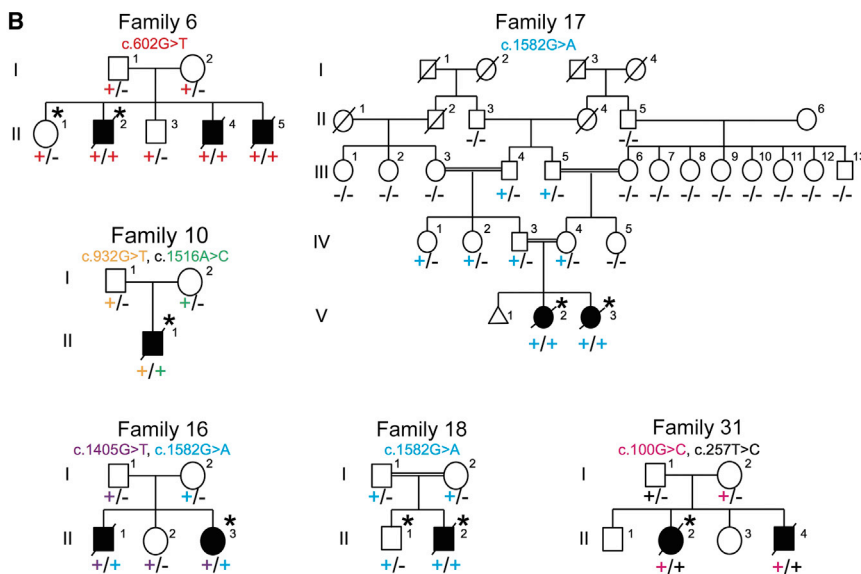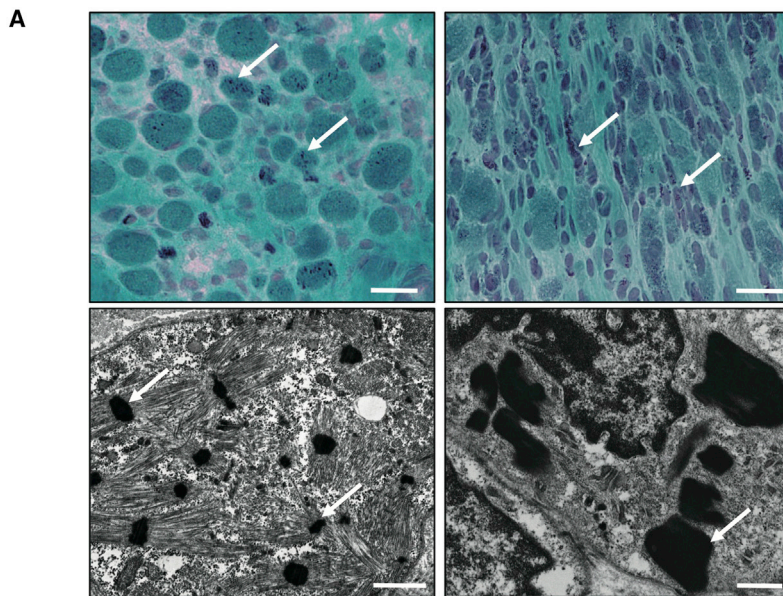
pathway.[10] Nevertheless, some forms of NEM remain genetically unsolved.

One such subtype, which has long been recognized,[11,12] has apparent autosomal-recessive inheritance and is characterized by severe weakness, in utero presentation of fetal akinesia or hypokinesia and associated abnormalities, and muscle biopsy often showing numerous small nemaline bodies, sometimes only visible by electron microscopy and frequently with virtually no normal myofibrils remaining ("miliary NEM" Figure 1A and Figure S1, available online). We aimed to identify genetic causes of these severe NEM cases by using a combination of linkage analysis, or homozygosity mapping, SNP array, and whole-exome sequencing (WES) in selected families. We have identified loss-of-function mutations in *KLHL40* as a frequent cause of severe NEM and have shown through functional studies that KLHL40 is crucial for myogenesis and skeletal-muscle maintenance.

Subjects and Methods

Subject Details and Ethics

We recruited 143 genetically unresolved severe-NEM-affected families from large congenital-myopathy cohorts in major centers around the world (Boston, Helsinki, Perth, and Tokyo). All individuals within the cohorts were diagnosed with NEM on the basis of muscle-biopsy findings.

Written informed consent was obtained for participation in this study, which was approved by the Human Research Ethics

Introduction

Nemaline myopathy (NEM) is a common form of nondystrophic congenital myopathy and is defined clinically by skeletal-muscle dysfunction and pathologically by the presence of nemaline bodies within myofibers.[1,2] Typical clinical symptoms include hypotonia, muscle weakness of proximal dominance, respiratory insufficiency, and feeding problems. Congenital onset is usual, but a wide variation in age of onset and disease severity is recognized. Mutations in seven genes are known to cause NEM (NEM1–NEM7).[1,2] Six of these encode sarcomere-thin-filament proteins or associated proteins: *ACTA1* (MIM 102610),[3] *CFL2* (MIM 601443),[4] *NEB* (MIM 161650),[5] *TNNT1* (MIM 191041),[6] *TPM2* (MIM 190990),[7] and *TPM3* (MIM 191030);[8] the seventh, *KBTBD13* (kelch-repeat- and BTB-[POZ]-domain-containing 13 [MIM 613727])[9] is involved in the ubiquitin proteasome

Committee of the University of Western Australia (UWA), the ethics committee of the Children's Hospital of the University of Helsinki, Yokohama City University School of Medicine, and the Boston Children's Hospital institutional review board. The UWA Animal Ethics Committee approved animal studies.

Microscopy

Light microscopy and electron microscopy of biopsies was performed as previously described.[13]

Whole-Genome SNP Genotyping, Linkage Analysis, and WES

Genotyping was performed for families 6 and 18 with the use of the HumanOmniExpress BeadChip Kit (Illumina) and Infinium II Assay Workflow (Illumina) at the Institute for Molecular Medicine Finland (FIMM). Data were analyzed with PLINK v.1.07. Multiple large homozygous regions were identified, but none included known myopathy-associated genes. WES was performed on one healthy and one affected sibling from family 6 and the proband from family 18 with the SeqCap EZ Human Exome Library v.2.0 exome system (Nimblegen, Roche Diagnostics). Coverage depths were 31- to 62-fold. Variant quantification was performed with the FIMM Variant Calling Pipeline v.1.0 and the Integrative Genomics Viewer (IGV, Broad Institute of MIT and Harvard). All known and heterozygous SNPs were excluded. Healthy siblings' genotypes were used for the exclusion of shared homozygous variants.

Five individuals from family 16 were genotyped with the Human Mapping 10K XbaI 142 2.0 array (Affymetrix) and GeneChip Genotyping Analysis Software (Gtypev4.1). Parametric linkage analysis was performed with Allegro v.2 with a fully penetrant autosomal-recessive model. WES was performed on the proband with the use of the SureSelect Human All Exon 50 Mb Kit (Agilent Technologies) and sequenced in one lane on a GAIIx platform (Illumina) with 108 bp paired-end reads. Reads were aligned to the UCSC Genome Browser (GRCh37/hg19) with Novoalign (Novocraft Technologies). Mean coverage depth was 59-fold. Single-nucleotide variants and small indels were identified with GATK UnifiedGenotyper and filtered according to the Broad Institute's Best Practices guidelines v.3. Variants registered in dbSNP132 were filtered. The filter-passed variants were annotated with ANNOVAR. Only genes with homozygous variants or more than two variants located in the candidate linkage regions were included.

Family 17 was genotyped with the HumanCytoSNP-12 BeadChip (Illumina). MERLIN was used for performing linkage analysis on a subset of 14,514 SNPs.[14] WES was performed for the proband from family 10 and for both siblings from family 17 as described.[15] Coverage depth was 61- to 97-fold. Variants were called with LifeScope 2.5 (Life Technologies) and filtered with ANNOVAR[16] against ENCODE GENCODE v.11 (October 2011 freeze, GRCh37).[17] Two custom variant-filtering steps were used: (1) one against the 1000 Genomes database (February 2012 release) (variants with a minor allele frequency > 0.5% were excluded) and (2) one against the dbSNP135 common database.

Family 31 (BOS74) was one in a cohort of 59 NEM-affected families who underwent WES by the Intellectual and Developmental Disabilities Research Center Core Next-Gen Sequencing Facility of Boston Children's Hospital and Harvard Medical School in collaboration with Axeq Technologies, Complete Genomics, Integrated Genetics (LabCorp), and the Boston Children's Hospital Gene Partnership. Exome sequencing was performed with the Illumina HiSeq 2000 platform. Reads were mapped with the Burrows-Wheeler Aligner (v.0.5.8). SNPs and indels were called with SAMtools (v.0.1.7). Data analysis and variant calling were performed with the Broad GATK Best Practices for identification of SNPs and small indels. Annotated variants were filtered against dbSNP135, the 1000 Genomes Project database (October 2011 edition), and the National Heart, Lung, and Blood Institute (NHLBI) Exome Sequencing Project Exome Variant Server (EVS).

Sequencing

Bidirectional Sanger sequencing of *KLHL40* (RefSeq accession number NM_152393.2) was performed on biobanked DNA from additional probands with severe NEM and their family members in Boston, Helsinki, Perth, Yokohama, and Tokyo. Identified variants were then screened in all available family members. Primer sequences and conditions are available upon request. For detection of the c.1582G>A (p.Glu528Lys) mutation in normal Japanese controls, high-resolution melting (HRM) analysis with and without the spike-in method[18] was performed on LightCycler 480 System II (Roche Diagnostics). If samples showed any aberrant melting patterns, Sanger sequencing was performed for confirmation of the mutation.

LOD Scores

Where possible, MERLIN was used for calculating LOD scores for individual families.[14]

Expression Analysis on Human cDNAs

TaqMan quantitative real-time PCR analyses were performed with cDNAs of human adult (Human MTCPanel I, #636742, Clontech Laboratories) and fetal (Human Fetal MTC Panel, #636747, Clontech Laboratories) tissues.[19] Predesigned TaqMan probe sets for human *KLHL40* (*KBTBD5*, Hs00328078_m1, Applied Biosystems) and human β-actin (*ACTB*, 4326315E, Applied Biosystems) were used. PCR was performed on a Rotor-Gene Q (QIAGEN) (conditions are available upon request) and analyzed with the Rotor-Gene Q Series Software by the $2^{-\Delta\Delta Ct}$ method. Relative concentrations of cDNA were normalized to concentrations obtained from the hearts.

Calculations of the Free-Energy Change upon Amino Acid Substitutions

Molecular structures were drawn with PyMOL. FoldX v.3.0 beta[20] was used through a graphics interface as a plugin for the YASARA molecular viewer.[21] Crystal structures of the kelch domain of human KLHL40 (Protein Data Bank [PDB] code 4ASC) and the BTB (bric-a-brac, tram-track, broad-complex)-BACK (BTB and C-terminal kelch) domain of human KHLH11 (PDB code 3I3N) were energy-minimized with the RepairPDB command implemented in FoldX and subsequently with the BuildModel command for mutagenesis. Protein stabilities were calculated by the Stability command, and the free-energy changes were estimated by subtraction of the free-energy value of the wild-type protein from those of the altered proteins. The procedure was repeated three times for each substitution, and the resultant data were presented as an average value with SDs.

Immunoblotting and Immunohistochemistry

SDS-PAGE and immunoblotting were performed as described.[22,23] For protein studies, C2C12 myoblasts and myotubes were grown and prepared for immunoblotting and immunofluorescence as

described.[23] For KLHL40 immunoblots, the Human Protein Atlas (HPA) rabbit polyclonal KLHL40 (KBTBD5) antibody from Sigma was used (HPA024463 [1:2,500 dilution]). Immunostaining of human and mouse muscle samples was performed as described[13,23] with a KLHL40 antibody (KBTBD5; HPA024463 [1:100 dilution]).

Zebrafish Studies

In Situ Hybridization
Digoxigenin probes for *klhl40a* and *klhl40b* were generated by cDNA amplification of 1,340 and 694 bp sequences, respectively (Table S1). In situ hybridizations were performed as described previously.[24]

Morpholino Microinjection
Antisense translation-blocking morpholinos (Table S1) for *klhl40a* (*klhl40a*-MO) and *klhl40b* (*klhl40b*-MO and *klhl40b*-MO2) were coinjected into 1- to 2-cell-stage embryos at a final concentration of 0.25 or 0.5 mM. Morpholino efficacies were tested by immuno-blotting for Klhl40.

Zebrafish Immunohistochemistry
Immunohistochemistry of zebrafish embryos was performed as described[24,25] with myosin heavy chain (MHC) antibody (F59 [1:20 dilution] or A4.1025 [1:10 dilution]; Developmental Studies Hybridoma Bank) and α-actinin (1:100 dilution; Sigma) and fila-min C (1:100 dilution; Sigma) antibodies, and Alexa-Fluor-488-conjugated phalloidin (1:100 dilution; Molecular Probes) was used for labeling F-actin. Immunoreactivity was detected with an Alexa-Fluor-594-conjugated anti-mouse secondary antibody diluted in blocking buffer (1:200).

Statistical Analyses
Statistical analyses of clinical features were carried out with SPSS Statistics 19 (IBM) software. Individuals for whom information for a clinical feature was not available were excluded from the analysis of that feature. Either Chi-square tests or Fisher's exact tests were applied for comparing each phenotypic variable between different genotypes. $p < 0.05$ was considered statistically significant.

Results

WES identified homozygous or compound-heterozygous mutations in *KLHL40* (kelch-like family member 40; also known as *KBTBD5* [kelch-repeat- and BTB-(POZ)-domain-containing 5] and *SYRP* [sarcosynapsin]) in six NEM-affected families (families 6, 10, 16–18, and 31; Figure 1B and Table 1). Subsequent screening of *KLHL40* by Sanger sequencing in additional probands with severe NEM resulted in the identification of a total of 19 variants (4 frameshifts, 12 missense mutations, 2 nonsense mutations, and 1 splice site) in 28 (19.6%) apparently unrelated families (Table 1) from the cohort of 143 families affected by severe NEM. In addition, 129 probands with milder NEM were screened, but no *KLHL40* mutations were identified in this cohort, confirming that *KLHL40* mutations are most likely exclusive to cases of severe NEM.

In all cases where it was possible to test unaffected parents, siblings, and extended family, the mutations cosegregated with disease in an autosomal-recessive fashion (Figure 1B), giving a combined LOD score of 5.66 (Table 1). All mutations were either absent from the NHLBI EVS and the 1000 Genomes database[26] or present at low frequencies in the heterozygous state (Table 1). In five additional NEM-affected families, only single *KLHL40* variants were identified (Table S2); the significance of these variants in these individuals remains unclear.

In Japanese persons, *KLHL40* mutations are the most common cause of this severe form of NEM (13/47 [~28%]) as a result of a founder effect with the c.1582G>A mutation. Given that this mutation was present in Turkish, Kurdish, and Japanese families, we completed a haplotype analysis of Japanese and Turkish families (families 16 and 17) but did not identify a common haplotype between them (Figure S2). HRM with confirmatory Sanger sequencing of 510 normal Japanese individuals revealed a heterozygous c.1582G>A mutation in one individual. Therefore, the mutant-allele frequency in the Japanese population was estimated to be 0.0098. According to the equation described by Kimura and Ota[27] and under the assumption of 25 years per generation, the age of this mutation is calculated to be 4,900 years old.

The identified *KLHL40* mutations were scattered throughout all exons (Table 1 and Figure 2A) encoding mostly conserved residues (Figure S3). To investigate disease mechanisms, all substitutions except p.Arg311Leu were mapped to the crystal structures of the kelch domain of human KLHL40 and the BTB-BACK domain of human kelch-like protein 11 (KLHL11; Figures 2B and 2C and Figure S4). p.Arg311Leu (c.932G>T) was predicted to be in the structurally flexible region, a linker of nonconserved amino acids connecting the BACK and kelch domains (Figure S7D), and was therefore excluded from structural consideration. All the modeled substituted residues are involved in intramolecular interactions, and thus the substitutions would most likely destabilize the hydrophobic cores of the BTB-BACK domain (p.Leu86Pro [c.257T>C], p.Val194Glu [c.581T>A], and p.Trp201Leu [c.602G>A]), the kelch domain (p.Pro397Leu [c.1190C>T], p.His455Arg [c.1364A>G], and p.Gly469Cys [c.1405G>T]), the β sheet (p.Thr506Pro [c.1516A>C] and p.Ala538Pro [c.1612G>C]), or the hydrogen bonds between the main chain and side chain (p.Asp34His [c.100G>C] and p.Glu528Lys [c.1582G>A]) or between side chains (p.Glu588Lys [c.1762G>A]) (Figures S5–S7). The p.Pro397Leu and p.Glu588Lys substitutions appear to be conservative for the hydrophobic core and hydrogen bonding, respectively. The former substitution is predicted to affect the polyproline II helix conformation (residues 396–399; Figure S6A). The calculated free-energy change for most substitutions was estimated to be over 2.0 kcal/mol (Figure 2D), which is typically associated with destabilization of domain folds.[28] These analyses suggested that most *KLHL40* missense mutations impair protein stability.

To investigate *KLHL40* expression and KLHL40 abundance, we performed quantitative RT-PCR and immunoblotting of human and mouse tissues. *KLHL40* transcripts

Table 1. *KLHL40* Mutations by Family, Individual LOD Scores, Ethnicity, and Population-wide Incidence

Family	Exon(s)	Mutation		LOD Score	Ethnicity	Incidence from EVS (1st; 2nd)	Incidence from 1000 Genomes (1st; 2nd)
		Nucleotide Change	Amino Acid Change				
Family 31[a]	1	c.[100G>C];[257T>C]	p.[Asp34His];[Leu86Pro]	0.6	Vietnamese	ND; ND	ND; ND
Family 2	1	c.[134delC];[134delC]	p.[Pro45Argfs*19]; [Pro45Argfs*19]	NA	Italian	NA	ND
Family 3	1	c.[270C>G];[270C>G]	p.[Tyr90*];[Tyr90*]	NA	Turkish	ND	ND
Family 5	1	c.[581T>A];[581T>A]	p.[Val194Glu];[Val194Glu]	0.6	Israeli	ND	ND
Family 6[a]	1	c.[602G>T];[602G>T]	p.[Trp201Leu];[Trp201Leu]	1.454	Turkish	ND	ND
Family 7	1	c.[602G>A];[602G>A]	p.[Trp201*];[Trp201*]	NA	Norwegian	ND	ND
Family 9	1	c.[790delC];[790delC]	p.[Arg264Alafs*59]; [Arg264Alafs*59]	0.25	Turkish	NA	ND
Family 10[a]	1 and 4	c.[932G>T];[1516A>C]	p.[Arg311Leu];[Thr506Pro]	NA	Chinese	ND; ND	ND; ND
Family 34	2 and 6	c.[1190C>T];[1762G>A]	p.[Pro397Leu];[Glu588Lys]	NA	Turkish	ND; ND	ND; A = 2 and G = 2,184
Family 12	2 and 4	c.[1270_1272delinsAGATC AAGGT];[1582G>A]	p.[Asp424Argfs*23]; [Glu528Lys]	NA	Japanese	NA; ND	ND; ND
Family 13	2 and 4	c.[1281_1294delCTGCCTGG ACTCGG];[1582G>A]	p.[Cys428Hisfs*12]; [Glu528Lys]	NA	Korean	NA; ND	ND; ND
Family 14	3	c.[1364A>G];[1364A>G]	p.[His455Arg];[His455Arg]	NA	Turkish	ND	ND
Family 15	3	c.[1405G>T];[1405G>T]	p.[Gly469Cys];[Gly469Cys]	NA	Japanese	ND	ND
Family 16[a]	3 and 4	c.[1405G>T];[1582G>A]	p.[Gly469Cys];[Glu528Lys]	0.727	Japanese	ND; ND	ND; ND
Family 17[a]	4	c.[1582G>A];[1582G>A]	p.[Glu528Lys];[Glu528Lys]	1.654	Turkish	ND	ND
Family 18[a]	4	c.[1582G>A];[1582G>A]	p.[Glu528Lys];[Glu528Lys]	0.125	Kurdish	ND	ND
Family 19	4	c.[1582G>A];[1582G>A]	p.[Glu528Lys];[Glu528Lys]	0.25	Kurdish	ND	ND
Family 20	4	c.[1582G>A];[1582G>A]	p.[Glu528Lys];[Glu528Lys]	NA	Japanese	ND	ND
Family 21	4	c.[1582G>A];[1582G>A]	p.[Glu528Lys];[Glu528Lys]	NA	Japanese	ND	ND
Family 22	4	c.[1582G>A];[1582G>A]	p.[Glu528Lys];[Glu528Lys]	NA	Japanese	ND	ND
Family 23	4	c.[1582G>A];[1582G>A]	p.[Glu528Lys];[Glu528Lys]	NA	Japanese	ND	ND
Family 24	4	c.[1582G>A];[1582G>A]	p.[Glu528Lys];[Glu528Lys]	NA	Japanese	ND	ND
Family 25	4	c.[1582G>A];[1582G>A]	p.[Glu528Lys];[Glu528Lys]	NA	Japanese	ND	ND
Family 26	4	c.[1582G>A];[1582G>A]	p.[Glu528Lys];[Glu528Lys]	NA	Japanese	ND	ND
Family 27	4	c.[1582G>A];[1582G>A]	p.[Glu528Lys];[Glu528Lys]	NA	Japanese	ND	ND
Family 28	4	c.[1582G>A];[1582G>A]	p.[Glu528Lys];[Glu528Lys]	NA	Japanese	ND	ND
Family 29	4/5	c.[1608−1G>A];[1608−1G>A]	NA	NA	Turkish	ND	ND
Family 30	5	c.[1612G>C];[1612G>C]	p.[Ala538Pro];[Ala538Pro]	NA	Turkish	ND	ND

The individual pedigree LOD scores are given where possible. This table also shows the incidence of the mutations reported within the NHLBI EVS and the 1000 Genomes browser. Abbreviations are as follows: NA, not available; and ND, not detected.
[a]Families for whom WES was performed.

and their encoded proteins were exclusive to developing and adult skeletal muscle (Figures 3A–3C) and more abundant in fetal muscle than in postnatal muscle (Figure 3C). Confocal microscopy suggested that KLHL40 might localize to the sarcomeric A-band (Figure 3D and Figure S8), a region not previously linked to NEM. Immunoblotting showed that KLHL40 is absent or of low abundance in *KLHL40*-associated NEM muscle (Figure 3E), even for persons harboring two missense mutations (F10 and F17). Immunohistochemistry confirmed that KLHL40 was absent or very scarce in *KLHL40*-associated NEM myofibers (Figure 3F).

We further investigated Klhl40 function in zebrafish. The zebrafish genome contains two orthologs of *KLHL40*: *klhl40a* and *klhl40b*, which have 57% (*klhl40a*) and 55.7% (*klhl40b*) amino acid similarity to human KLHL40. RT-PCR demonstrated expression of both *klhl40* genes at 24 and 48 hr postfertilization (hpf) (Figure S9A). In adult
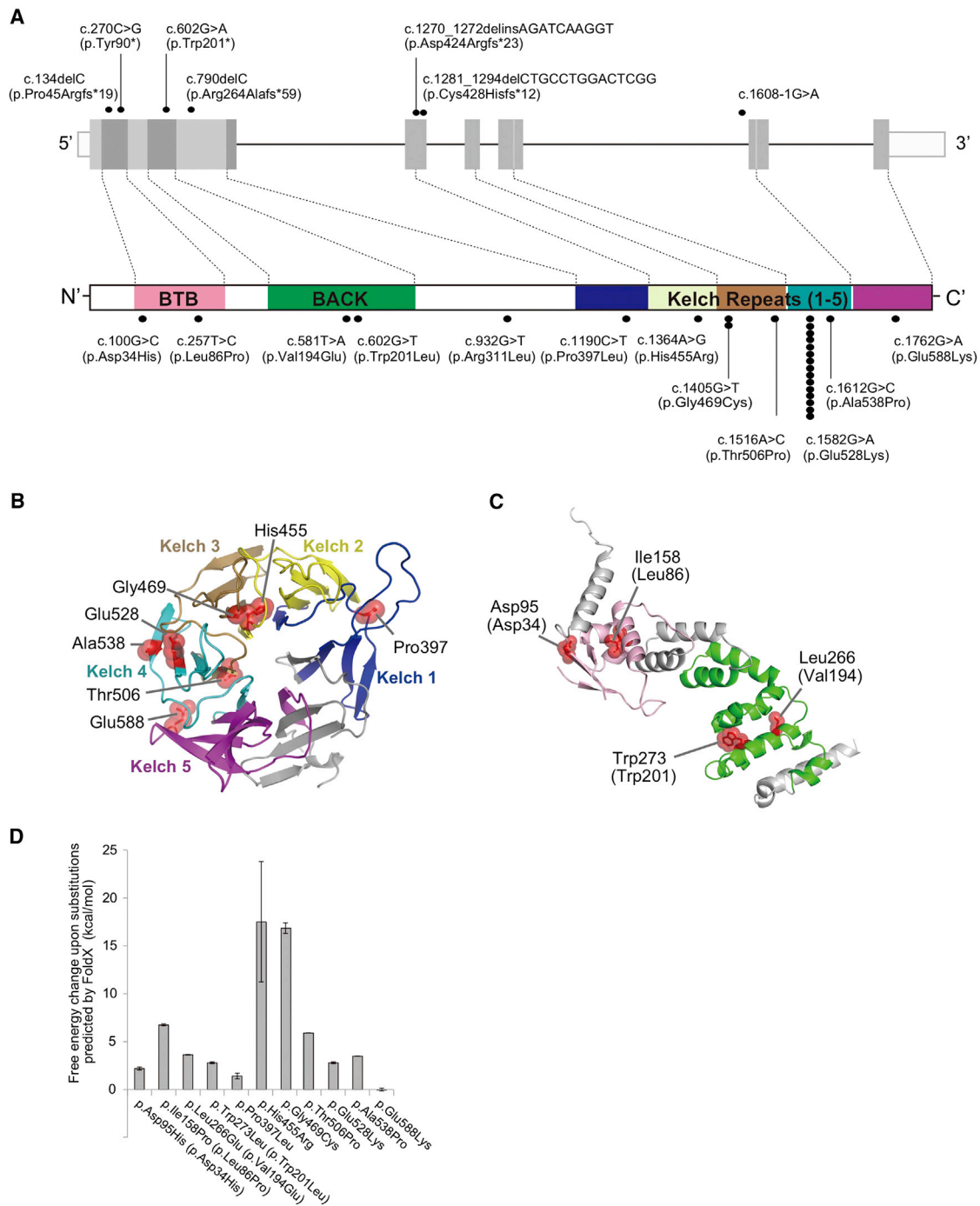
Figure 2. Mutations Identified in Our Cohort and the Structural Modeling of the Missense KLHL40 Substitutions

(A) Schematic presentation of the genomic structure of *KLHL40* (upper) and its encoded protein, KLHL40, with the BTB-BACK domain and kelch repeats (lower). The localization of mutations and substitutions identified is depicted with dots, and the number of dots for each mutation or substitution indicates the number of times it was found. Most substitutions occurred at conserved amino acids. The dots above *KLHL40* indicate truncating mutations, and those below *KLHL40* indicate missense mutations.

(B and C) Structural modeling of the missense KLHL40 substitutions. The crystal structures of the (B) kelch domain of KLHL40 and the (C) BTB-BACK domain of KLHL11 and the location of the substitutions are shown. p.Pro397Leu, p.His455Arg, p.Glu469Cys, p.Thr506Pro, p.Glu528Lys, p.Ala538Pro, and p.Glu588Lys map to the kelch repeats (B), p.Asp34His and p.Leu86Pro map to the BTB domain, and p.Val194Lys and p.Trp201Leu map to the BACK domain (C). The side chains of the mutated residues are shown as sticks with space-filling spheres in red. α helices, β sheets, and loops are drawn as ribbons, arrows, and threads, respectively. Each kelch repeat (B) is color coded in the kelch domain, and the BTB and BACK domains (C) are colored pink and green, respectively. Molecular structures were drawn with PyMOL.

(D) The calculated free-energy changes resulting from the missense substitutions in the kelch domain of human KLHL40 and the BTB-BACK domain of human KLHL11 were predicted by FoldX. Data are presented as the mean ± SD. Residue numbers used in (C) and (D) refer to human KLHL11, and those corresponding to human KLHL40 are in parentheses.
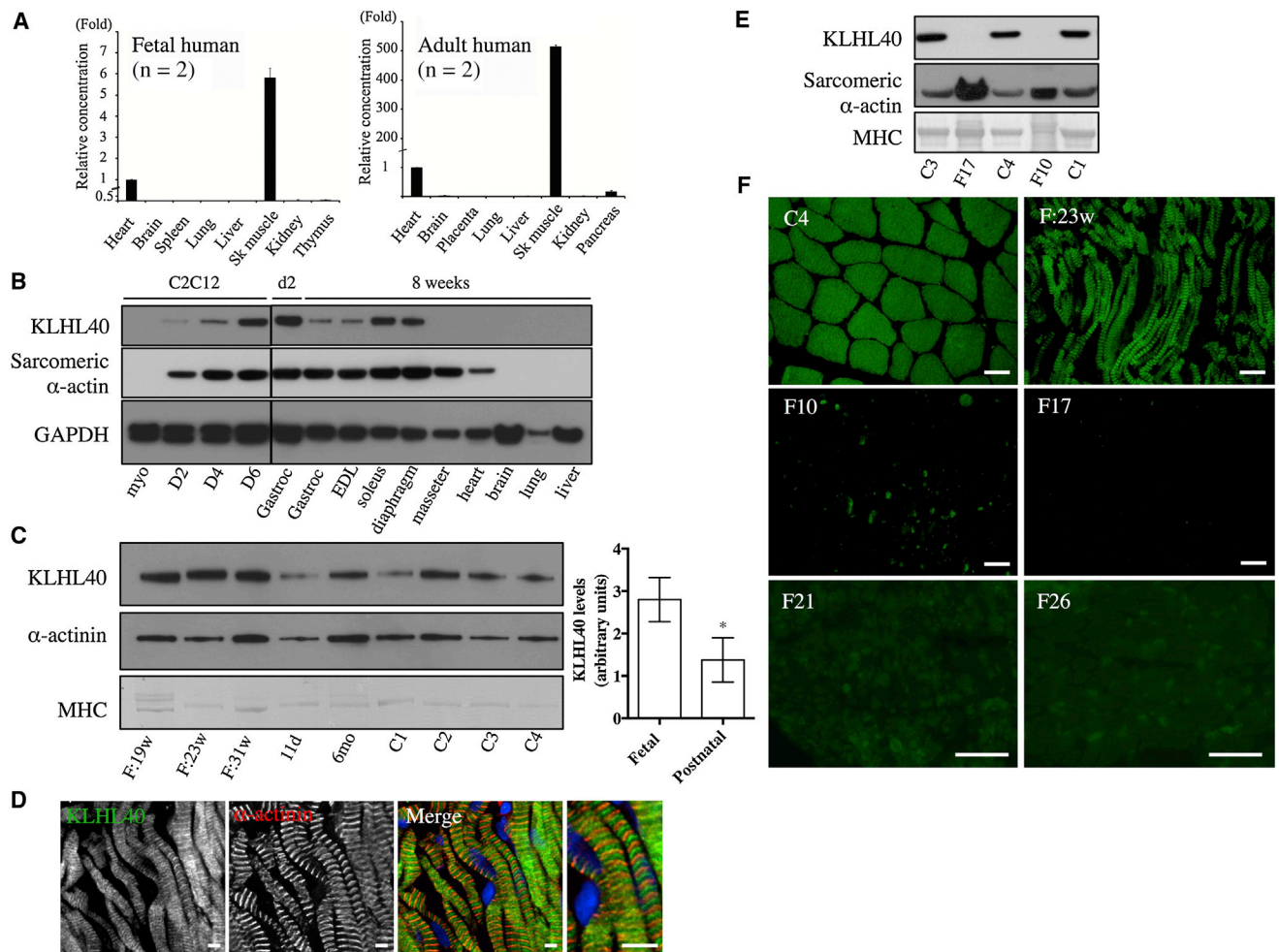
Figure 3. *KLHL40* Expression in Human and Mouse Tissues

(A) Taqman quantitative real-time PCR analysis of cDNA from adult or fetal human tissues. Error bars represent the SD. The following abbreviation is used: Sk, skeletal.

(B) KLHL40 levels in C2C12 cells and mouse tissues (HPA, top panel) and immunoblotting for sarcomeric α-actin (clone 5C5, middle panel) and GAPDH (lower panel). Lanes are as follows: myo, C212 myoblasts; D2, myotubes on day 2 of differentiation; D4, myotubes on day 4 of differentiation; D6, myotubes on day 6 of differentiation; Gastroc (left), C57BL/6 postnatal day 2 (d2) gastrocnemius; Gastroc (right), C57BL/6 8-week-old gastrocnemius; and EDL (extensor digitorum longus) to liver, C57BL/6 8-week-old tissues. For all mouse tissue lysates, samples were pooled from three different mice.

(C) On the left is KLHL40 expression in human skeletal muscle (HPA, top panel), immunoblotting for α-actinin (clone EA-53, middle panel), and Coomassie staining of MHC band (bottom panel). Lanes are as follows: F:19w, 19-week-old fetus; F:23w, 23-week-old fetus; F:31w, 31-week-old fetus; 11d, 11-day-old neonate; 6mo, 6-month-old baby; and C1–C4, healthy adult controls of 19–42 years of age. On the right, KLHL40 intensity normalized to MHC for fetal muscle is 3.34 ± 0.92 ($n = 3$) versus 1.37 ± 0.21 ($n = 6$) for postnatal skeletal muscle. *$p = 0.023$, unpaired two-tailed t test. Error bars represent the SEM.

(D) Single Z-plane confocal microscopy showing localization of KLHL40 (green) and α-actinin (red) in a longitudinal section of skeletal muscle from a 31-week-old fetus; costaining with Hoechst (blue) is also shown (Merge). Scale bars represent 5 μm.

(E) Immunoblotting shows that KLHL40 is absent in *KLHL40*-associated NEM muscle (II-1 from family 10 [F10] and V-2 from family 17 [F17]) compared with healthy control muscle (C1, C3, and C4). Coomassie staining of the MHC band (bottom panel) and immunoblotting for sarcomeric α-actin (clone 5C5, middle panel) indicate similar or greater loading for the *KLHL40*-associated NEM samples compared with control samples.

(F) Immunofluorescence for KLHL40 in a human 23-week-old fetal skeletal muscle sample (F:23w), an adult healthy control (C4), and *KLHL40*-associated NEM muscle biopsies (II-1 from family 10 [F10], V-2 from family 17 [F17], family 21 [F21], and family 26 [F26]). Scale bars represent 50 μm.

zebrafish, *klhl40a* was most abundant in the skeletal muscle and heart and *klhl40b* was most abundant in the skeletal muscle (Figure S9A). At the 16 and 24 hpf stages, expression of both genes was restricted to the muscle precursor cells in the somites (Figure 4A). We knocked down zebrafish *klhl40a* and *klhl40b* with antisense morpholino oligonucleotides (*klhl40a*-MO, *klhl40b*-MO, and *klhl40b*-MO2) (Figures S9B and S10A). Embryos injected with *klhl40a*-MO, *klhl40b*-MO, and *klhl40a*-MO/*40b*-MO (double morpholinos) showed a curved trunk and small head at 48 hpf (Figures 4B and 4C). A normal phenotype resulted from 5 bp mismatched morpholinos (5mis-MOs).
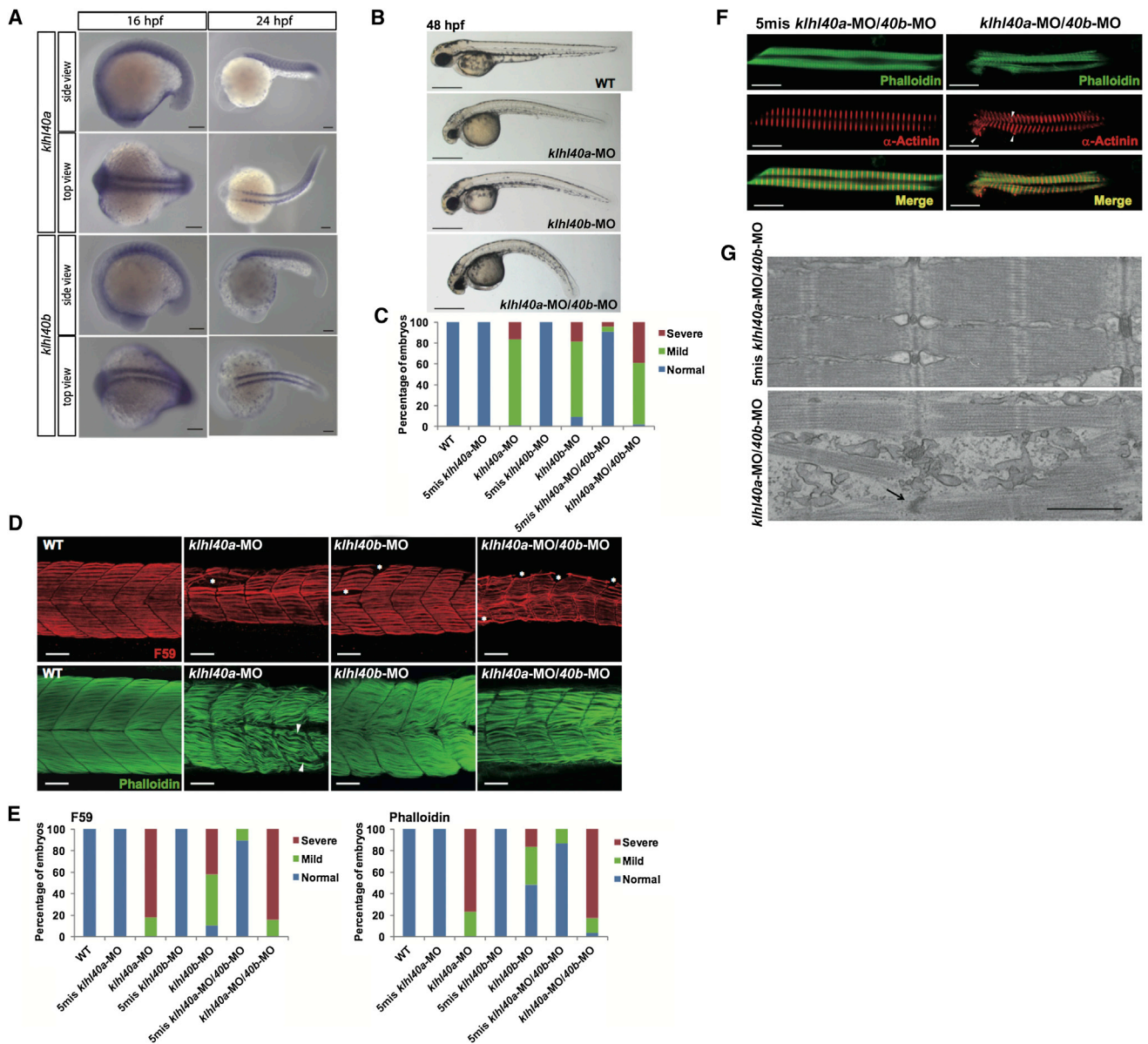
Figure 4. Expression and Function of *klhl40* in Zebrafish

(A) In situ hybridization demonstrates that expression of both *klhl40a* and *klhl40b* is restricted to the skeletal muscle at 16 and 24 hpf.

(B) Gross morphology of uninjected embryos (WT) and embryos injected with *klhl40a*-MO, *klhl40b*-MO, and *klhl40a*-MO/*40b*-MO. Lateral views of MO-injected embryos (4 ng) at 48 hpf are shown. Scale bars represent 500 μm.

(C) Percentage of embryos categorized in phenotypic classes after injection with the 5mis-MO control, *klhl40a*-MO, *klhl40b*-MO, or *klhl40a*-MO/*40b*-MO. We categorized the phenotypes at 48 hpf into normal (normal appearance), mild (curved trunk), and severe (tail defect and severe development delay) (n = 111–130).

(D) Knockdown of *klhl40a*, *klhl40b*, or both resulted in severe disruption of the skeletal muscle: fibers appeared wavy, and there were extensive gaps between fibers in contrast to the densely packed and aligned fibers of the controls. Maximum-intensity projection images from a confocal image series followed immunolabeling with a myosin antibody (F59, upper panels) at 36 hpf and F-actin (lower panels) at 72 hpf.

(E) Embryos injected with 5mis-MO, *klhl40a*-MO, *klhl40b*-MO, or *klhl40a*-MO/*40b*-MO were categorized phenotypically on the basis of the presence of myofiber detachment affecting one to two somites (mild) or multiple (three or more) somites (severe) (n = 25–44).

(F) Double-labeled immunofluorescence was performed on isolated myofibers from 72 hpf embryos with the use of phalloidin (green) and α-actinin (red). Frequent areas of aberrant α-actinin accumulation were detected in *klhl40a*-MO/*40b*-MO myofibers (arrowheads).

(G) Electron microscopy of 72 hpf myofibers. A 5mis-MO-injected embryo shows correctly aligned sarcomeres and T-tubules (upper panel). A *klhl40a*-MO/*40b*-MO-injected embryo (lower panel) shows disarranged myofibrils with widened Z-disks (arrow), but thin filament lengths are unchanged. The scale bar represents 0.7 μm.

We analyzed slow myofibers in more detail by immuno-staining slow myosin heavy chains (Figure 4D, upper panels). *klhl40* morphants showed disruption of muscle patterning with an irregular, wavy appearance of the stri-ated myofibers and extensive gaps between the myofibers (Figures 4D and 4E and Figure S10B) and a greatly

Table 2. Summary of Clinical Features of NEM Individuals with *KLHL40* Mutations

	Individuals with *KLHL40* Mutations (n = 32 Cases from 28 Families)	
	Total	**Percentage**
Family history	17/28	60.7%
Consanguinity	10/28	35.7%
Prenatal Period		
Prenatal symptoms	24/29	82.8%
Fetal akinesia or hypokinesia	16/21	76.2%
Polyhydramnios	14/29	48.3%
Neonatal Period		
Respiratory function		
respiratory failure	28/29	96.6%
requiring ventilation	11/29	37.9%
Facial involvement	26/26	100%
weakness	23/23	100%
ophthalmoparesis	4/23	17.4%
mild dysmorphology	15/15	100%
Dysphagia	23/24	95.8%
with tube feeding or gastrostomy	13/24	54.2%
Muscle weakness	29/29	100.0%
with no spontaneous antigravity movements	13/29	44.8%
Contracture(s)	24/27	88.9%
Pathological fracture(s)	10/19	52.6%
Average age at death	5 months (n = 14)	
Average gestation age at birth	37 weeks (n = 27)	
Average birth weight	2,558 g (n = 26)	

Total numbers were calculated as the number of individuals with the clinical features over the total number of individuals whose medical records were available for each category.

diminished birefringence (Figure S10C). Isolated myofibers from *klhl40a*-MO/*40b*-MO fish, coimmunostained with phalloidin and an α-actinin antibody (Z-disk), showed disorganized and irregular patterns with small aggregates of α-actinin, suggesting nemaline bodies (Figure 4F). Aggregation of Z-disk material was also confirmed by immunostaining for filamin C in *klhl40a*-MO/*40b*-MO fish (Figure S11). Electron-microscopic analysis revealed disarranged myofibrils with widened Z-disks (Figure 4G). Fish injected with *klhl40a*-MO, *klhl40b*-MO, *klhl40b*-MO2, or *klhl40a*-MO/*40b*-MO2 (double morpholinos) exhibited sporadic muscle tremors, and coordinated swimming behavior was not observed (Movies S1 and S2). These results suggest that Klhl40a and Klhl40b are required for muscle development and function and that loss of either isoform in the early embryo is sufficient to impair normal mobility.

Detailed clinical records were collected and analyzed for 32 affected individuals from the 28 unrelated kindreds afflicted with *KLHL40* mutations. These individuals were from various ethnicities, such as European, Middle and Near Eastern, or Asian. Clinical features of individuals with *KLHL40* mutations were severe and distinctive (Table 2 and Table S3). Eighty-three percent of affected individuals showed prenatal symptoms, and 76% displayed fetal akinesia or hypokinesia. Most persons had severe respiratory compromise (97%), and approximately a third required ventilatory support (38%). Almost all affected individuals (96%) also had swallowing problems, and half required tube feeding or gastrostomy. Muscle weakness was severe. Forty-five percent of individuals had no spontaneous antigravity movement. Seventeen percent of affected individuals were also noted to have ophthalmoparesis, a relatively rare symptom in NEM. Multiple joint contractures and pathological bone fracture were other common features. Dysmorphic facial features and deformities of the chest, spine, fingers, and feet were also frequent. The average age of death was 5 months. Many families, including a previously described family (family 30 herein, cases 2–6 in Lammens et al.),[11] were consanguineous.

We further evaluated whether there are any genotype-phenotype correlations in *KLHL40*-associated NEM. We compared the clinical features of individuals according to the type of mutation they had (either two truncating mutations, one truncating mutation and one missense mutation, or two missense mutations) and the pattern of mutations (homozygous or compound heterozygous). No significant differences in frequencies of these clinical features were observed (data not shown). We also compared the clinical features of persons with the recurrent c.1582G>A genotype (either with this mutation [genotype G/A or A/A as group A] or without [genotype G/G as group G]). Prenatal symptoms, including fetal akinesia or hypokinesia, were frequently observed (73.3% in group A versus 92.9% in group G). Respiratory failure was common in both groups (100% in group A versus 92.9% in group G), but there were significantly fewer individuals requiring ventilation in group A than in group G (20.0% in group A versus 57.1% in group G; p = 0.047). Dysphagia was also common in both groups (100% in group A versus 90.0% in group G), but there were fewer persons requiring tube feeding or gastrostomy in group A than in group G, although the difference was not significant (42.9% in group A versus 70.0% in group G; p = 0.127). Facial weakness was observed in all affected individuals in both groups, but fewer individuals in group A had ophthalmoparesis (7.7% in group A versus 30.0% in group G; p = 0.281). All persons also had muscle weakness, but significantly fewer individuals in group A had the most severe form of muscle weakness with no antigravity movements (20.0% in group A versus 71.4% in group G; p = 0.018). Significantly fewer affected individuals in group A were deceased at the time of study than in group G (23.5% in group A versus 71.4% in group G; p = 0.012;

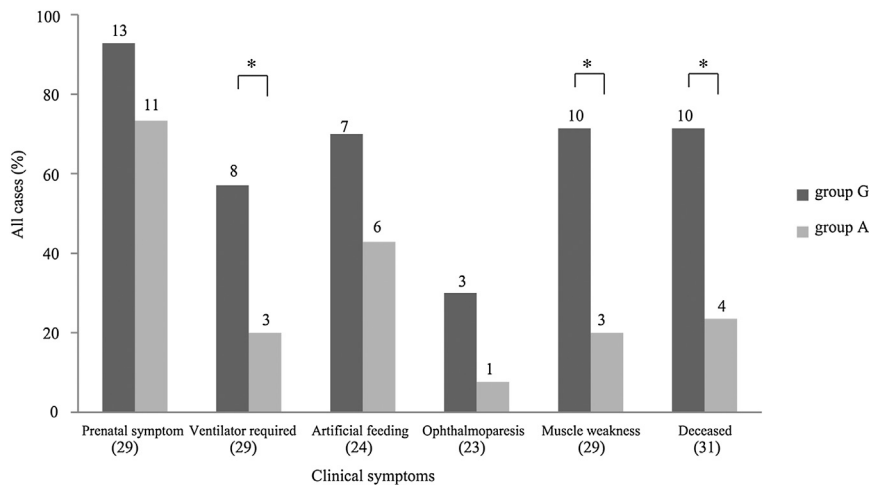**Figure 5. Correlation between the c.1582G>A (p.Glu528Lys) Mutation and Clinical Features**

The clinical characteristics of NEM are shown for the two groups of affected individuals (32 total), either with the c.1582G>A (p.Glu528Lys) mutation (as group A) or without it (as group G). The numbers of total affected individuals with clinical records regarding either the presence or the absence of each characteristic are indicated below the bars, and the numbers of affected individuals in each group are indicated above the respective bars. Labels on the x axis are as follows: prenatal symptoms, individuals demonstrating either fetal akinesia or hypokinesia, polyhydramnios, or fetal edema or effusion; ventilator required, individuals with respiratory failure requiring ventilation; artificial feeding, dysphagia-affected persons requiring tube feeding or gastrostomy; ophthalmoparesis, individuals with ophthalmoparesis along with facial weakness; muscle weakness, individuals with the most severe form of muscle weakness and demonstrating no antigravity movement; and deceased, individuals who were deceased at the time of study. Asterisks indicate that statistical significance was observed.

odds ratio = 8.125; 95% confidence interval = 1.62–40.75) (Figure 5). We further compared the clinical features of individuals of different ethnicities (either European or Asian descent) according to the c.1582G>A genotype, and similar tendencies were demonstrated (data not shown). There was, however, great variation in severity for individuals with or without the c.1582G>A genotype.

Discussion

We have described the identification of recessive *KLHL40* mutations in individuals with severe NEM from 28 unrelated families of various ethnicities. The c.1582G>A mutation was the most frequently detected mutation and was found in Japanese, Kurdish, and Turkish persons. However, comparison of haplotypes between a Japanese family and a Turkish family suggested that the mutation arose independently in these ethnic groups. We have shown several lines of evidence of the pathogenicity of the *KLHL40* mutations. The missense mutations occurred mostly in conserved functional domains within KLHL40, and they were predicted to destabilize the intramolecular interactions and thus impair protein stability. This was corroborated by the absence of KLHL40 even in the skeletal muscle of individuals harboring two missense mutations. We have established a locus-specific database for *KLHL40* mutations at the Leiden Muscular Dystrophy Pages.

Expression of KLHL40 in fetal and adult skeletal muscle indicates that KLHL40 plays a role in both myogenesis and mature muscle. KLHL40 appears to be more abundant in fetal skeletal muscle than in postnatal skeletal muscle and most likely accounts for the prevalence of in utero presentations in this NEM cohort. Perhaps KLHL40 is more important for myogenesis than for muscle maintenance; this could account for the fact that the disease ranges so

much in severity, from some individuals' dying within hours of being born to others' surviving into adolescence. Our zebrafish studies have demonstrated that Klhl40a and Klhl40b are not required for the specification of muscle cells but rather for muscle patterning and function and that loss of either isoform in the early embryo is sufficient to impair normal mobility, supporting the involvement of KLHL40 in NEM-associated fetal akinesia. It has previously been suggested that KLHL40 is also important for muscle maintenance through the process of degeneration and regeneration.[29,30] *Klhl40* is upregulated in myogenic precursors after cardiotoxin injury of mouse skeletal muscle, supporting a role for *Klhl40* in the response to muscle damage.[29] Studies of cattle muscle have shown increased *Klhl40* expression in another catabolic process, undernutrition, further suggesting a role for *KLHL40* in the stress response.[30]

KLHL40 belongs to the superfamily of kelch-repeat-containing proteins that form characteristic β-propeller structures,[31] which bind substrate proteins and are involved in a wide variety of functions. In humans, 71 kelch-repeat-containing proteins have been identified.[31] The majority contain an N-terminal BTB domain (also known as the POZ [poxvirus and zinc finger] domain) and a BACK motif. Proteins containing both a BTB domain and a kelch repeat have previously been implicated in neuromuscular disease. A dominant *KLHL9* mutation causes an early-onset distal myopathy (distal myopathy 1 [MIM 160500]),[32] and dominant *KBTBD13* mutations cause nemaline myopathy with cores (MIM 609273).[9] We now show that *KLHL40*, encoding KLHL40, which contains both a BTB domain and a kelch repeat, is associated with autosomal-recessive neuromuscular disease. BTB domains function as substrate-specific adaptors for cullin 3 (Cul3),[33,34] a component of the E3-ubiquitin-ligase complex. Both KLHL9 and KBTBD13 bind Cul3.[10,32] MuRF1,

an E3-ubiquitin ligase, is known to be recruited to M-line titin and is thought to modulate myofibrillar turnover and the trophic state of muscle.[35] KLHL40 appears to be present at the A-band and might be similarly involved through the ubiquitin-proteasome pathway.

We have characterized the severe and distinctive features of this disease as fetal akinesia or hypokinesia during the prenatal period, respiratory failure and swallowing difficulty at birth, contractures and fractures along with dysmorphic features, and in most cases, early death. We have also shown that persons with the recurrent c.1582G>A mutation tend to have relatively milder symptoms compared to those of individuals without c.1582G>A. However, the severity of the disease in persons with or without the c.1582G>A genotype varied greatly (for example, from death at 20 days to still being alive at 11 years for persons homozygous for the c.1582G>A genotype), suggesting modifying factors.

Fetal akinesias are clinically and genetically heterogeneous, and the majority of cases still remain genetically unsolved.[36] Primary muscle diseases account for up to 50% of such syndromes.[37] On the basis of our study, *KLHL40* mutations cause a significant proportion of severe NEM cases of fetal akinesia sequence and the disease shows worldwide prevalence. *KLHL40* should be considered when a clinician encounters an individual presenting with prenatal symptoms, such as fetal akinesia or hypokinesia, or clinical features and/or pathology of severe NEM at birth (especially miliary NEM, which was present in at least 20% of our *KLHL40*-mutation cases), along with an autosomal-recessive pattern of family history. Fractures are a relatively frequent presentation within this cohort, unlike other NEM cohorts, and should also be used for directing genetic screening of *KLHL40*. We show that KLHL40 immunohistochemistry, immunoblotting, or genetic screening will identify the disease and thus allow genetic counseling for the affected individual's family.

In conclusion, this study associates loss-of-function *KLHL40* mutations with severe, often in utero, NEM. Many probands who do not harbor *KLHL40* mutations present with NEM in utero, suggesting further genetic heterogeneity. Clarification of KLHL40 function and interactions might lead to a greater understanding of the pathogenesis of disease, the identification of other candidates for this severe form of NEM, and the investigation of possible therapies.

Supplemental Data

Supplemental Data include 11 figures, three tables, and two movies and can be found with this article online at http://www.cell.com/AJHG.

Acknowledgments

Web Resources

The URLs for data presented herein are as follows:

1000 Genomes Project, http://www.1000genomes.org/
dbSNP, http://www.ncbi.nlm.nih.gov/projects/SNP/
Leiden Open Variation Database, www.LOVD.nl/KLHL40
NHLBI Exome Sequencing Project (ESP) Exome Variant Server, http://evs.gs.washington.edu/EVS/
Online Mendelian Inheritance in Man (OMIM), http://www.omim.org
PyMOL, http://www.pymol.org
RefSeq, http://www.ncbi.nlm.nih.gov/RefSeq

References

1. Nance, J.R., Dowling, J.J., Gibbs, E.M., and Bönnemann, C.G. (2012). Congenital myopathies: an update. Curr. Neurol. Neurosci. Rep. *12*, 165–174.
2. Nowak, K.J., Davis, M.R., Wallgren-Pettersson, C., Lamont, P.J., and Laing, N.G. (2012). Clinical utility gene card for: nemaline myopathy. Eur. J. Hum. Genet. *20*. Published online April 18, 2012. http://dx.doi.org/10.1038/ejhg.2012.70.
3. Nowak, K.J., Wattanasirichaigoon, D., Goebel, H.H., Wilce, M., Pelin, K., Donner, K., Jacob, R.L., Hübner, C., Oexle, K., Anderson, J.R., et al. (1999). Mutations in the skeletal muscle alpha-actin gene in patients with actin myopathy and nemaline myopathy. Nat. Genet. *23*, 208–212.
4. Agrawal, P.B., Greenleaf, R.S., Tomczak, K.K., Lehtokari, V.L., Wallgren-Pettersson, C., Wallefeld, W., Laing, N.G., Darras,

B.T., Maciver, S.K., Dormitzer, P.R., and Beggs, A.H. (2007). Nemaline myopathy with minicores caused by mutation of the CFL2 gene encoding the skeletal muscle actin-binding protein, cofilin-2. Am. J. Hum. Genet. *80*, 162–167.

5. Lehtokari, V.L., Pelin, K., Sandbacka, M., Ranta, S., Donner, K., Muntoni, F., Sewry, C., Angelini, C., Bushby, K., Van den Bergh, P., et al. (2006). Identification of 45 novel mutations in the nebulin gene associated with autosomal recessive nemaline myopathy. Hum. Mutat. *27*, 946–956.

6. Johnston, J.J., Kelley, R.I., Crawford, T.O., Morton, D.H., Agarwala, R., Koch, T., Schäffer, A.A., Francomano, C.A., and Biesecker, L.G. (2000). A novel nemaline myopathy in the Amish caused by a mutation in troponin T1. Am. J. Hum. Genet. *67*, 814–821.

7. Donner, K., Ollikainen, M., Ridanpää, M., Christen, H.J., Goebel, H.H., de Visser, M., Pelin, K., and Wallgren-Pettersson, C. (2002). Mutations in the beta-tropomyosin (TPM2) gene—a rare cause of nemaline myopathy. Neuromuscul. Disord. *12*, 151–158.

8. Laing, N.G., Wilton, S.D., Akkari, P.A., Dorosz, S., Boundy, K., Kneebone, C., Blumbergs, P., White, S., Watkins, H., Love, D.R., et al. (1995). A mutation in the alpha tropomyosin gene TPM3 associated with autosomal dominant nemaline myopathy. Nat. Genet. *9*, 75–79.

9. Sambuughin, N., Yau, K.S., Olivé, M., Duff, R.M., Bayarsaikhan, M., Lu, S., Gonzalez-Mera, L., Sivadorai, P., Nowak, K.J., Ravenscroft, G., et al. (2010). Dominant mutations in KBTBD13, a member of the BTB/Kelch family, cause nemaline myopathy with cores. Am. J. Hum. Genet. *87*, 842–847.

10. Sambuughin, N., Swietnicki, W., Techtmann, S., Matrosova, V., Wallace, T., Goldfarb, L., and Maynard, E. (2012). KBTBD13 interacts with Cullin 3 to form a functional ubiquitin ligase. Biochem. Biophys. Res. Commun. *421*, 743–749.

11. Lammens, M., Moerman, P., Fryns, J.P., Lemmens, F., van de Kamp, G.M., Goemans, N., and Dom, R. (1997). Fetal akinesia sequence caused by nemaline myopathy. Neuropediatrics *28*, 116–119.

12. Lacson, A.G., Donaldson, G., Barness, E.G., Ranells, J.D., and Pomerance, H.H. (2002). Infant with high arched palate, bell-shaped chest, joint contractures, and intrauterine fractures. Pediatr. Pathol. Mol. Med. *21*, 569–584.

13. Ravenscroft, G., Jackaman, C., Bringans, S., Papadimitriou, J.M., Griffiths, L.M., McNamara, E., Bakker, A.J., Davies, K.E., Laing, N.G., and Nowak, K.J. (2011). Mouse models of dominant ACTA1 disease recapitulate human disease and provide insight into therapies. Brain *134*, 1101–1115.

14. Abecasis, G.R., Cherny, S.S., Cookson, W.O., and Cardon, L.R. (2002). Merlin—rapid analysis of dense genetic maps using sparse gene flow trees. Nat. Genet. *30*, 97–101.

15. Ravenscroft, G., Thompson, E.M., Todd, E.J., Yau, K.S., Kresoje, N., Sivadorai, P., Friend, K., Riley, K., Manton, N.D., Blumbergs, P., et al. (2013). Whole exome sequencing in foetal akinesia expands the genotype-phenotype spectrum of GBE1 glycogen storage disease mutations. Neuromuscul. Disord. *23*, 165–169.

16. Wang, K., Li, M., and Hakonarson, H. (2010). ANNOVAR: functional annotation of genetic variants from high-throughput sequencing data. Nucleic Acids Res. *38*, e164.

17. Harrow, J., Denoeud, F., Frankish, A., Reymond, A., Chen, C.K., Chrast, J., Lagarde, J., Gilbert, J.G., Storey, R., Swarbreck, D., et al. (2006). GENCODE: producing a reference annotation for ENCODE. Genome Biol. *7*(*Suppl 1*), S4.1–S4.9.

18. Garritano, S., Gemignani, F., Voegele, C., Nguyen-Dumont, T., Le Calvez-Kelm, F., De Silva, D., Lesueur, F., Landi, S., and Tavtigian, S.V. (2009). Determining the effectiveness of High Resolution Melting analysis for SNP genotyping and mutation scanning at the TP53 locus. BMC Genet. *10*, 5.

19. Doi, H., Yoshida, K., Yasuda, T., Fukuda, M., Fukuda, Y., Morita, H., Ikeda, S., Kato, R., Tsurusaki, Y., Miyake, N., et al. (2011). Exome sequencing reveals a homozygous SYT14 mutation in adult-onset, autosomal-recessive spinocerebellar ataxia with psychomotor retardation. Am. J. Hum. Genet. *89*, 320–327.

20. Schymkowitz, J., Borg, J., Stricher, F., Nys, R., Rousseau, F., and Serrano, L. (2005). The FoldX web server: an online force field. Nucleic Acids Res. *33*(Web Server issue), W382–W388.

21. Van Durme, J., Delgado, J., Stricher, F., Serrano, L., Schymkowitz, J., and Rousseau, F. (2011). A graphical interface for the FoldX forcefield. Bioinformatics *27*, 1711–1712.

22. Nowak, K.J., Ravenscroft, G., Jackaman, C., Filipovska, A., Davies, S.M., Lim, E.M., Squire, S.E., Potter, A.C., Baker, E., Clément, S., et al. (2009). Rescue of skeletal muscle alpha-actin-null mice by cardiac (fetal) alpha-actin. J. Cell Biol. *185*, 903–915.

23. Ravenscroft, G., Nowak, K.J., Jackaman, C., Clément, S., Lyons, M.A., Gallagher, S., Bakker, A.J., and Laing, N.G. (2007). Dissociated flexor digitorum brevis myofiber culture system—a more mature muscle culture system. Cell Motil. Cytoskeleton *64*, 727–738.

24. Ruparelia, A.A., Zhao, M., Currie, P.D., and Bryson-Richardson, R.J. (2012). Characterization and investigation of zebrafish models of filamin-related myofibrillar myopathy. Hum. Mol. Genet. *21*, 4073–4083.

25. Zeller, J., Schneider, V., Malayaman, S., Higashijima, S., Okamoto, H., Gui, J., Lin, S., and Granato, M. (2002). Migration of zebrafish spinal motor nerves into the periphery requires multiple myotome-derived cues. Dev. Biol. *252*, 241–256.

26. Abecasis, G.R., Auton, A., Brooks, L.D., DePristo, M.A., Durbin, R.M., Handsaker, R.E., Kang, H.M., Marth, G.T., and McVean, G.A.; 1000 Genomes Project Consortium. (2012). An integrated map of genetic variation from 1,092 human genomes. Nature *491*, 56–65.

27. Kimura, M., and Ota, T. (1973). The age of a neutral mutant persisting in a finite population. Genetics *75*, 199–212.

28. Guerois, R., Nielsen, J.E., and Serrano, L. (2002). Predicting changes in the stability of proteins and protein complexes: a study of more than 1000 mutations. J. Mol. Biol. *320*, 369–387.

29. Embree, E.J. (2007). The identification and characterization of MKRP, a novel kelch related protein. PhD Thesis, Graduate School of Biomedical Sciences, The University of Texas Southwestern Medical Center at Dallas, Dallas, TX. http://repositories.tdl.org/utswmed-ir/bitstream/handle/2152.5/226/embreelaurence.pdf?sequence=3.

30. Lehnert, S.A., Byrne, K.A., Reverter, A., Nattrass, G.S., Greenwood, P.L., Wang, Y.H., Hudson, N.J., and Harper, G.S. (2006). Gene expression profiling of bovine skeletal muscle in response to and during recovery from chronic and severe undernutrition. J. Anim. Sci. *84*, 3239–3250.

31. Prag, S., and Adams, J.C. (2003). Molecular phylogeny of the kelch-repeat superfamily reveals an expansion of BTB/kelch proteins in animals. BMC Bioinformatics *4*, 42.

32. Cirak, S., von Deimling, F., Sachdev, S., Errington, W.J., Herrmann, R., Bönnemann, C., Brockmann, K., Hinderlich, S.,

Lindner, T.H., Steinbrecher, A., et al. (2010). Kelch-like homologue 9 mutation is associated with an early onset autosomal dominant distal myopathy. Brain *133*, 2123–2135.

33. Furukawa, M., He, Y.J., Borchers, C., and Xiong, Y. (2003). Targeting of protein ubiquitination by BTB-Cullin 3-Roc1 ubiquitin ligases. Nat. Cell Biol. *5*, 1001–1007.

34. Canning, P., Cooper, C.D., Krojer, T., Murray, J.W., Pike, A.C., Chaikuad, A., Keates, T., Thangaratnarajah, C., Hojzan, V., Marsden, B.D., et al. (2013). Structural basis for Cul3 protein assembly with the BTB-Kelch family of E3 ubiquitin ligases. J. Biol. Chem. *288*, 7803–7814.

35. Mrosek, M., Labeit, D., Witt, S., Heerklotz, H., von Castelmur, E., Labeit, S., and Mayans, O. (2007). Molecular determinants for the recruitment of the ubiquitin-ligase MuRF-1 onto M-line titin. FASEB J. *21*, 1383–1392.

36. Ravenscroft, G., Sollis, E., Charles, A.K., North, K.N., Baynam, G., and Laing, N.G. (2011). Fetal akinesia: review of the genetics of the neuromuscular causes. J. Med. Genet. *48*, 793–801.

37. Quinn, C.M., Wigglesworth, J.S., and Heckmatt, J. (1991). Lethal arthrogryposis multiplex congenita: a pathological study of 21 cases. Histopathology *19*, 155–162.